## Piezoelectric effect and diode effect in anapole and monopole superconductors

Michiya Chazono,<sup>1,\*</sup> Shota Kanasugi,<sup>1</sup> Taisei Kitamura,<sup>1</sup> and Youichi Yanase<sup>1</sup>

\*Department of Physics, Kyoto University, Kyoto 606-8502, Japan

(Dated: December 27, 2022)

Superconductors lacking both inversion symmetry and time-reversal symmetry have been attracting much attention as a platform for exotic superconducting phases and anomalous phenomena, including the superconducting diode effect. Recent studies revealed intrinsic phases with this symmetry, named anapole superconductivity and monopole superconductivity, which are PT-symmetric superconducting states with and without Cooper pairs' total momentum, respectively. To explore characteristic phenomena in these states, we calculate and predict the superconducting piezoelectric effect and superconducting diode effect. A close relationship with the finite-q pairing, asymmetric Bogoliubov spectrum, and quantum geometry is discussed. This study reveals the piezoelectric and diode effects as potential probes to elucidate exotic superconducting phases.

#### I. INTRODUCTION

In recent years, superconductors lacking both inversion symmetry (IS) and time-reversal symmetry (TRS) are received much attention. For instance, nonreciprocal charge responses are extensively studied in superconductors with such symmetry [1–9]. Especially, the superconducting diode effect has become a central topic in condensed matter physics, and vast experimental and theoretical studies are conducted [10–26]. These nonreciprocal phenomena are expected to be ubiquitous since the simultaneous breaking of IS and TRS can be realized in various situations. Superconductors with noncentrosymmetric crystal structures under magnetic fields are typical examples [1-5, 10-12, 18-22, 25, 26]. Spontaneous breaking of TRS symmetry due to magnetism also results in the superconducting diode effect [15, 16, 23]. Furthermore, we can utilize the supercurrent that breaks both IS and TRS without dissipation [6, 7].

In the recent study [27], an intrinsic mechanism of spontaneous IS and TRS breaking is predicted for one of the multiple superconducting phases in UTe<sub>2</sub> [28–34]. The competing instability of spin-triplet and spin-singlet superconductivity causes spontaneous parity mixing of Cooper pairs. In the centrosymmetric crystals such as UTe<sub>2</sub>, the phase difference between the even-parity and odd-parity pair potentials is likely to be  $\pm \pi/2$  [35], leading to the IS and TRS breaking with intact PT-symmetry in the mixed-parity superconducting state. The PTsymmetric superconducting state is a novel quantum condensed phase of matter, and the realization in UTe<sub>2</sub> and other exotic superconductors is attracting attention. Therefore, it is eagerly desired to clarify the unique properties of the PT-symmetric superconducting states and to explore possible probes of them.

Let us classify the *PT*-symmetric superconducting states. In analogy with the *PT*-symmetric magnetic order [36], they are classified into monopole, anapole, quadrupole, and higher-order multipole superconducting

states. An intriguing class is the anapole superconductivity, where Cooper pairs can get finite total momentum at zero magnetic field [37, 38]. The anapole superconducting state is distinguished by the Fulde-Ferrell-Larkin-Ovchinnikov (FFLO) state [39, 40] and the helical superconducting state [41, 42] which require finite magnetic field or spin polarization. In the anapole superconductors, the finite-q pairing state is characterized by a polar vector named the effective anapole moment, which was recently revealed to arise from various origins [37, 38]. On the other hand, the other classes of PT-symmetric superconducting states are nonpolar, and Cooper pairs condensate with zero total momentum. An example of them appears in the classification table for UTe<sub>2</sub> (Table III), named (magnetic) monopole superconductivity. The analysis of the periodic Anderson model has shown that both anapole and monopole superconducting states are candidate superconducting states of UTe<sub>2</sub> [27].

An important consequence of the IS and TRS breaking is the asymmetric spectrum of Bogoliubov quasiparticles, which arises from the multiband effects in anapole and monopole superconductors [37, 38]. In principle, we can distinguish all the PT-symmetric superconducting phases by the asymmetric profile of the Bogoliubov spectrum. However, the direct measurement of the Bogoliubov spectrum is challenging, especially for low-temperature superconductors. Thus, we are motivated to explore the macroscopic phenomena of anapole and monopole superconductors, especially those allowed only when symmetry breaking occurs.

For this purpose, in this paper, we study the superconducting piezoelectric effect (SCPE), a supercurrent-induced lattice distortion that occurs only when the superconductors lack both IS and TRS. We have investigated the SCPE in two-dimensional helical superconductors [43], where TRS is broken by an external magnetic field. This paper focuses on the SCPE in the anapole and monopole superconductors, where IS and TRS are broken by spontaneous parity mixing in Cooper pairs without noncentrosymmetric crystal structure or external field. We also investigate the superconduct-

<sup>\*</sup> chazono.michiya.84s@st.kyoto-u.ac.jp

ing diode effect (SDE) and predict the intrinsic SDE in the anapole superconducting state, although it is absent in the monopole superconducting state. As a link of the SCPE and SDE with Cooper pairs' momentum was shown in the helical superconductors [18-20, 25, 43], we also discuss the properties of finite-q pairing in the anapole superconducting state for comparison. It is shown that the SCPE shows distinct behaviors depending on the origin of finite-q pairing, namely, the asymmetric Bogoliubov spectrum and quantum geometry [37, 38].

This paper is organized as follows. In Sec. II, we show a minimal model for the anapole and monopole superconducting states introduced in the previous study [37] and formulate the SCPE based on the model. We also introduce the classification of possible PT-symmetric superconducting states in UTe<sub>2</sub>. In Sec. III, we show numerical results of the SCPE coefficients and Cooper pairs' momentum. It is revealed that the SCPE occurs in both anapole and monopole superconducting states. The behaviors of the SCPE are closely related to the origin of the effective anapole moment, which causes finite-q pairing. We demonstrate the SDE in Sec. IV as another anomalous phenomenon in the anapole superconductors. In Sec. V, we summarize our study and discuss the future outlook.

#### II. FORMULATION

# A. Minimal model for anapole and monopole superconducting states

We adopt a minimal model for the anapole and monopole superconducting states, which was introduced in the previous study for UTe<sub>2</sub> [37]. While UTe<sub>2</sub> has a centrosymmetric crystal structure with  $D_{2h}$  point group symmetry, the IS is locally broken on U sites owing to the sublattice degree of freedom. Using the Nambu spinor  $\hat{c}_{\mathbf{k}}^T = (c_{\mathbf{k}1\uparrow}, c_{\mathbf{k}2\uparrow}, c_{\mathbf{k}1\downarrow}, c_{\mathbf{k}2\downarrow})$  where 1, 2  $(\uparrow, \downarrow)$  denote the sublattice (spin) degree of freedom, we write the Bogoliubov-de Gennes (BdG) Hamiltonian in the following form:

$$\mathcal{H}_{\boldsymbol{q}} = \frac{1}{2} \sum_{\boldsymbol{k}} (\hat{c}_{\boldsymbol{k}+\boldsymbol{q}}^{\dagger} \ \hat{c}_{-\boldsymbol{k}+\boldsymbol{q}}^{T}) H_{\text{BdG}}(\boldsymbol{k}, \boldsymbol{q}) \begin{pmatrix} \hat{c}_{\boldsymbol{k}+\boldsymbol{q}} \\ \hat{c}_{-\boldsymbol{k}+\boldsymbol{q}}^{*} \end{pmatrix}, \quad (1)$$

$$H_{\mathrm{BdG}}(\boldsymbol{k},\boldsymbol{q}) = \begin{pmatrix} H_0(\boldsymbol{k}+\boldsymbol{q}) & \Delta(\boldsymbol{k})(i\sigma_y \otimes \tau_0) \\ (\Delta(\boldsymbol{k})(i\sigma_y \otimes \tau_0))^{\dagger} & -H_0(-\boldsymbol{k}+\boldsymbol{q})^T \end{pmatrix}, \quad (2)$$

where  $\tau$  ( $\sigma$ ) represents the Pauli matrix vector for the sublattice (spin) degree of freedom. We here assume Cooper pairs' total momentum 2q. Later, we show that q is finite in the anapole superconducting state while q=0 in the monopole superconducting state. The normal state Hamiltonian  $H_0(\mathbf{k})$  and superconducting order parameter  $\Delta(\mathbf{k})$  are defined as follows.

The sublattice degree of freedom with a locally noncentrosymmetric crystal structure allows the staggered antisymmetric spin-orbit coupling (ASOC) in the centrosymmetric materials [44]. Therefore, the normal state Hamiltonian is given by

$$H_0(\mathbf{k}) = (\varepsilon_{\mathbf{k}} - \mu)\sigma_0 \otimes \tau_0 + \mathbf{g}_{\mathbf{k}} \cdot \boldsymbol{\sigma} \otimes \tau_z, \tag{3}$$

where  $\varepsilon_{\mathbf{k}} = -2t(\cos k_x + \cos k_y + \cos k_z)$  is a kinetic energy and  $\mathbf{g}_{\mathbf{k}} = (\alpha_x \sin k_y, \ \alpha_y \sin k_x, \ 0)$  represents the ASOC. Note that the relation  $\alpha_y = -\alpha_x$  is not required because the local symmetry on U sites is orthorhombic  $C_{2v}$ , although it must be satisfied in the tetragonal  $C_{4v}$  systems.

We consider mixed-parity order parameters for the anapole and monopole superconducting states, and evenand odd-parity gap functions have  $\pi/2$  phase difference consistent with the thermodynamic stability [35]. Because of the locally noncentrosymmetric crystal structure [44], in addition to the conventional even-parity spin-singlet and odd-parity spin-triplet pairings, even-parity spin-triplet and odd-parity spin-singlet pairings can be finite. To satisfy the fermion's anti-commutation relation, the superconducting order parameter is given by

$$\Delta(\mathbf{k}) = \Delta_1(\psi_{\mathbf{k}}^g \sigma_0 \otimes \tau_0 + \beta \mathbf{d}_{\mathbf{k}}^g \cdot \boldsymbol{\sigma} \otimes \tau_z) + \Delta_2(\psi_{\mathbf{k}}^u \sigma_0 \otimes \tau_z + \mathbf{d}_{\mathbf{k}}^u \cdot \boldsymbol{\sigma} \otimes \tau_0),$$
(4)

where  $\psi_{\pmb{k}}^{g(u)}$  is an even-parity (odd-parity) spin-singlet component and  $d_{k}^{g(u)}$  is an even-parity (odd-parity) spintriplet component of the gap function. In this paper, we assume the even-parity component belonging to the  $A_g$  irreducible representation, specifically,  $\psi_k^g = 1$  and  $\mathbf{d}_k^g = (0, \sin k_x, 0)$ . For the odd-parity component,  $B_{3u}$ and  $A_u$  irreducible representations are examined. For simplicity,  $\psi_{\mathbf{k}}^{u} = 0$  is ignored, and we consider spin-triplet pairing with  $\mathbf{d}_{\mathbf{k}}^{u} = (0, 0, \sin k_{y})$  and  $\mathbf{d}_{\mathbf{k}}^{u} = (0, 0, \sin k_{z}),$ corresponding to the  $B_{3u}$  and  $A_u$  representations, respectively. We choose a real  $\Delta_1$  and a pure imaginary  $\Delta_2$  without loss of generality. The coexistent  $A_g + i B_{3u}$ state and  $A_q+iA_u$  state realize the anapole and monopole superconductivity, as discussed in the next subsection. These states are predicted in a microscopic analysis of the periodic Andeson model for UTe<sub>2</sub> [27]. However, the following results are expected to be general in the sense that the main conclusion for the SCPE and SDE applies to other representations, such as the  $A_q + iB_{1u}$ state, as well. For a later discussion, we introduce  $\beta$  as the strength of the staggered spin-triplet gap function allowed in locally noncentrosymmetric superconductors [44]. We will see that  $\beta$  is an important parameter for the superconducting properties.

#### B. Superconducting piezoelectric effect (SCPE)

The SCPE is defined as a lattice distortion induced by a supercurrent [43]. In the linear response regime, it is formulated as follows,

$$s_{ij} = d_{ijk}^{(SC)} J_k, (5)$$

TABLE I. List of the irreducible representations (IRs) of the  $C_{2v}$  point group  $(A_g + iB_{3u}$  anapole superconducting state) and corresponding strain  $s_{ij}$ , supercurrent  $J_k$ , and SCPE mode  $d_{ijk}^{(SC)}$ .

IR	Strain	Supercurrent	SCPE mode
$\overline{A_1}$	$s_{xx}, s_{yy}, s_{zz}$	$J_x$	$d_{xxx}^{(SC)} \ d_{yyx}^{(SC)} \ d_{zzx}^{(SC)}$
$\overline{A_2}$	$s_{yz}$	_	_
$B_1$	$s_{zx}$	$J_z$	$d_{zxz}^{(\mathrm{SC})}$
$B_2$	$s_{xy}$	$J_y$	$d_{xyy}^{ m (SC)}$

TABLE II. List of the IRs of the  $D_2$  point group  $(A_g + iA_u \text{ monopole superconducting state})$  and corresponding strain  $s_{ij}$ , supercurrent  $J_k$ , and SCPE mode  $d_{ijk}^{(SC)}$ .

IR	Strain	Supercurrent	SCPE mode
$\overline{A_1}$	$s_{xx}, s_{yy}, s_{zz}$	-	_
$B_1$	$s_{xy}$	$J_z$	$d_{xyz}^{(\mathrm{SC})}$
$B_2$	$s_{zx}$	$J_y$	$d_{zxy}^{(\mathrm{SC})}$
$B_3$	$s_{yz}$	$J_x$	$d_{yzx}^{(\mathrm{SC})}$

where  $s_{ij}$  is a strain tensor,  $d_{ijk}^{(SC)}$  is a SCPE coefficient, and  $J_k$  is a supercurrent. Because  $s_{ij}$  ( $J_k$ ) is a parity even (odd) and time-reversal even (odd) quantity,  $d_{ijk}^{(SC)}$  can be finite only in systems lacking both IS and TRS.

The structure of the SCPE tensor  $d_{ijk}^{(SC)}$  depends on the point group of the superconducting states. For a coefficient  $d_{ijk}^{(SC)}$  to be finite, corresponding  $s_{ij}$  and  $J_k$  must belong to the same irreducible representation. Let us consider the cases of our model. The point group of the  $A_q + iB_{3u}$  state is polar  $C_{2v}$ , while that of the  $A_q + iA_u$ state is nonpolar  $D_2$ . Thus, the former is the anapole superconducting state and the latter is the monopole superconducting state in analogy with the classification of magnetic states [45]. The classification of the strain  $s_{ij}$ and supercurrent  $J_k$  based on the  $C_{2v}$  and  $D_2$  point group is summarized in Table I and II, respectively. The SCPE modes allowed by symmetry are also shown in the tables. We show the classification of PT-symmetric superconducting states in Table III and see that all the PT-symmetric superconducting states belong to either  $C_{2v}$  or  $D_2$  point group in the orthorhombic  $D_{2h}$  system. Thus, the classification in Table I and II applies the other states as well, when we choose an appropriate two-fold rotation axis for  $C_{2v}$  (See Appendix A for the complete

For the estimation of the strain, we calculate the expectation values of the weighted density operator, which characterizes the modulation of the hopping parameters due to the distortion [36, 43]. Although the strain is proportional to the weighted density, we avoid calculating the proportionality coefficient because it strongly de-

TABLE III. Point group of the mixed-parity superconducting states in  $D_{2h}$  systems. For the  $C_{2v}$  point group, x, y and z denote the principal axis.

	$A_g$	$B_{1g}$	$B_{2g}$	$B_{3g}$
$A_u$	$D_2$	$C_{2v}(z)$	$C_{2v}(y)$	$C_{2v}(x)$
	$C_{2v}(z)$			
$B_{2u}$	$C_{2v}(y)$	$C_{2v}(x)$	$D_2$	$C_{2v}(z)$
$B_{3u}$	$C_{2v}(x)$	$C_{2v}(y)$	$C_{2v}(z)$	$D_2$

pends on material parameters, such as electron-phonon coupling and elastic modulus. The weighted density operator is defined as

$$\hat{n}_{ij} = \sum_{\mathbf{k}} (\hat{c}_{\mathbf{k}+\mathbf{q}}^{\dagger} \hat{c}_{-\mathbf{k}+\mathbf{q}}^{T}) n_{ij}(\mathbf{k}, \mathbf{q}) \begin{pmatrix} \hat{c}_{\mathbf{k}+\mathbf{q}} \\ \hat{c}_{-\mathbf{k}+\mathbf{q}}^{*} \end{pmatrix}, \quad (6)$$

$$n_{ij}(\mathbf{k}, \mathbf{q}) = \frac{1}{2} \begin{pmatrix} D_{ij}(\mathbf{k} + \mathbf{q}) \times I_4 & 0 \\ 0 & -D_{ij}(-\mathbf{k} + \mathbf{q}) \times I_4 \end{pmatrix}, \quad (7)$$

$$D_{ij}(\mathbf{k}) = \begin{cases} \cos k_i & (i=j) \\ \sin k_i \sin k_j & (i \neq j) \end{cases}, \tag{8}$$

and expectation values are calculated by

$$\langle \hat{n}_{ij} \rangle_{\text{eq}, \mathbf{q}}$$

$$= \frac{1}{V} \sum_{\mathbf{k}\alpha} [U^{\dagger}(\mathbf{k}, \mathbf{q}) n_{ij}(\mathbf{k}, \mathbf{q}) U(\mathbf{k}, \mathbf{q})]_{\alpha\alpha} f(E_{\alpha}(\mathbf{k}, \mathbf{q})), \quad (9)$$

where  $E_{\alpha}$  are eigenvalues of the Hamiltonian, Eq. (2)

$$E_{\alpha}(\mathbf{k}, \mathbf{q}) = [U^{\dagger}(\mathbf{k}, \mathbf{q}) H_{\text{BdG}}(\mathbf{k}, \mathbf{q}) U(\mathbf{k}, \mathbf{q})]_{\alpha\alpha}, \qquad (10)$$

and  $f(E) = (e^{E/T} + 1)^{-1}$  is the Fermi distribution function. We calculate the expectation value of the supercurrent in a similar way,

$$\langle \hat{J}_{k} \rangle_{\text{eq}, \mathbf{q}}$$

$$= \frac{1}{V} \sum_{\mathbf{k}\alpha} [U^{\dagger}(\mathbf{k}, \mathbf{q}) J_{k}(\mathbf{k}, \mathbf{q}) U(\mathbf{k}, \mathbf{q})]_{\alpha\alpha} f(E_{\alpha}(\mathbf{k}, \mathbf{q})), \quad (11)$$

where

$$J_k(\mathbf{k}, \mathbf{q}) = \frac{e}{2} \begin{pmatrix} \partial_{k_k} H_0(\mathbf{k} + \mathbf{q}) & 0 \\ 0 & -\partial_{k_k} H_0(-\mathbf{k} + \mathbf{q}) \end{pmatrix}. \quad (12)$$

Then, we redefine the SCPE coefficient  $d_{ijk}^{(SC)}$  by

$$d_{ijk}^{(SC)} = \lim_{q_k' \to 0} \frac{\langle \hat{n}_{ij} \rangle_{\text{eq}, \mathbf{q} + q_k'} - \langle \hat{n}_{ij} \rangle_{\text{eq}, \mathbf{q} - q_k'}}{\langle \hat{J}_k \rangle_{\text{eq}, \mathbf{q} + q_k'} - \langle \hat{J}_k \rangle_{\text{eq}, \mathbf{q} - q_k'}}, \tag{13}$$

where  $q'_k$  is Cooper pairs' momentum parallel to the supercurrent  $J_k$ .

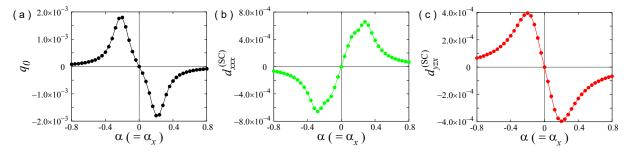


FIG. 1. Results of the group velocity model:  $\alpha(=\alpha_x)$  dependence of (a)  $q_0$ , (b)  $d_{xxx}^{(SC)}$  in the  $A_g+iB_{3u}$  anapole state, and (c)  $d_{yzx}^{(SC)}$  in the  $A_g+iA_u$  monopole state. We set  $\alpha_y=0,\ \beta=1$  and T=0.01.

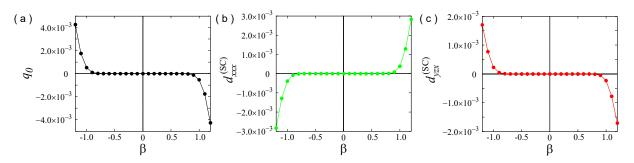


FIG. 2. Results of the group velocity model:  $\beta$  dependence of (a)  $q_0$ , (b)  $d_{xxx}^{(SC)}$  in the  $A_g + iB_{3u}$  anapole state, and (c)  $d_{yzx}^{(SC)}$  in the  $A_g + iA_u$  monopole state. We set  $\alpha_y = 0$ ,  $\alpha(=\alpha_x) = 0.4$  and T = 0.01.

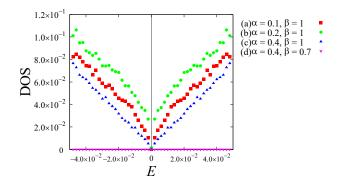


FIG. 3. The DOS in the group velocity model for the  $A_g + iB_{3u}$  anapole state. We set  $q_0 = 0$  for simplicity. The parameters are (a)  $\alpha = 0.1, \beta = 1$ , (b)  $\alpha = 0.2, \beta = 1$ , (c)  $\alpha = 0.4, \beta = 1$ , and (d)  $\alpha = 0.4, \beta = 0.7$ .

#### C. Classification of anapole superconducting states

In the previous section, the superconducting states have been classified based on symmetry. Here, we furthermore classify the anapole superconducting states by their microscopic properties.

The effective anapole moment in the superconducting state is defined by the first derivative of thermodynamic potential with respect to the Cooper pairs' momentum [37], and thus, finite anapole moment directly indicates the finite-q pairing state. As clarified in our recent work, there exist several origins of the effective anapole moment [38]. They are classified into the group velocity term and

the geometric term. While the former arises from the asymmetric Bogoliubov spectrum as pointed out in the previous study [37], the latter is induced by the quantum geometric effect, which recently attracts attention in various fields [46–61]. Owing to the geometric term, the finite-q pairing state can be stabilized even for ordinary electronic states, where neither the asymmetry nor the Zeeman splitting exists. Thus, the anapole superconducting states can be classified into three cases: The anapole moment is owing to (1) purely group velocity term, (2) purely geometric term, and (3) cooperation of the two terms.

The three cases can be represented in our model by choosing the following parameters:

- (1)  $\alpha_y = 0$  and  $\beta \neq 0$  (Group velocity model),
- (2)  $\alpha_y \neq 0$  and  $\beta = 0$  (Geometric effect model),
- (3)  $\alpha_y \neq 0$  and  $\beta \neq 0$  (Mixed model).

In the group velocity model, the group velocity term is finite while the geometric term vanishes. In contrast, the group velocity term vanishes in the geometric effect model. Both the group velocity and geometric terms are finite in the mixed model. In the next section, we show that the behaviors of the SCPE are different between the three cases.

In this study, we adopt the following parameters unless we explicitly state otherwise:  $t=1, \ \mu=-4, \ \Delta_1(T)=0.2\sqrt{1-(T/T_c)}, \ \Delta_2(T)=0.2i\sqrt{1-(T/T_c)}, \ (\text{namely}, \ |\Delta_2|=\Delta_1), \ \text{and the transition temperature is} \ T_c=0.1.$ 

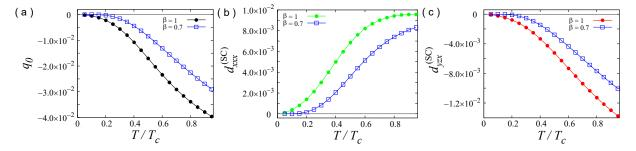


FIG. 4. Results of the group velocity model: temperature dependence of (a)  $q_0$ , (b)  $d_{xxx}^{(SC)}$  in the  $A_g + iB_{3u}$  anapole state, and (c)  $d_{yxx}^{(SC)}$  in the  $A_g + iA_u$  monopole state. We set  $\alpha_y = 0$ ,  $\alpha(= \alpha_x) = 0.4$  and  $\beta = 1$  or 0.7.

#### III. RESULT: SCPE

In this section, we show the numerical results of the Cooper pairs' momentum  $\mathbf{q}=(q_0,0,0)$ , the SCPE coefficient  $d_{xxx}^{(\mathrm{SC})}$  in the  $A_g+iB_{3u}$  anapole state, and  $d_{yzx}^{(\mathrm{SC})}$  in the  $A_g+iA_u$  monopole state. Because we find  $\mathbf{q}=0$  in the monopole state, we show  $q_0$  only for the anapole state. We discuss the  $\alpha(=\alpha_x)$ ,  $\beta$ , and T dependence of the SCPE in the three models introduced in the previous section (Sec. II C) and compare them with the Cooper pairs' momentum in the anapole superconducting state. A close relation between the SCPE and Cooper pairs' momentum is revealed.

#### (1) Group velocity model

First, we analyze the group velocity model, where we set  $\alpha_y=0$  and  $\beta\neq 0$ . In this model, the effect of the quantum geometry of Bloch states is negligible. The  $\alpha$  and  $\beta$  dependences of  $d_{ijk}^{(SC)}$  are shown in Figs. 1 and 2, together with the Cooper pairs' momentum  $q_0$  in the anapole state. It is shown that the SCPE coefficients are finite in the anapole and monopole superconducting states and their magnitudes are comparable. Thus, we see the SCPE in the PT-symmetric superconducting states, irrespective of whether the Cooper pairs' momentum is finite or zero.

On the other hand, we notice similarities between the SCPE and Cooper pairs' momentum by comparing the parameter dependence of  $d_{ijk}^{(\mathrm{SC})}$  and  $q_0$ . In particular, these quantities are antisymmetric with respect to  $\alpha$  and  $\beta$ . The antisymmetric behavior of  $q_0$  is expected from the result of the anapole moment  $T_x$  [38] because the relation  $q_0 \approx -T_x/D_{xx}$  holds with  $D_{xx}$  being the superfluid weight and  $T_x$  is  $\alpha$  ( $\beta$ ) antisymmetric in this model. On the other hand, it is nontrivial that  $d_{ijk}^{(\mathrm{SC})}$  is also antisymmetric. We can interpret the similarities by analogy with the magnetopiezoelectric effect [36, 62, 63], the counterpart of the SCPE in the normal state. It was shown that the magnetopiezoelectric effect originates from the asymmetric Fermi surface [36]. In the group velocity model, the Cooper pairs' momentum arises from the asymmetric

ric spectrum. Therefore, it is reasonable that the SCPE and Cooper pairs' momentum show similar behaviors. Indeed, their antisymmetric behaviors with respect to  $\alpha$  and  $\beta$  are explained as follows. The Bogoliubov spectrum is asymmetric and it is reversed by changing the sign of  $\alpha$  or  $\beta$  in this model (see Appendix B). Since the SCPE and Cooper pairs' momentum are caused by the asymmetric spectrum, it is natural that reversing spectrum changes the sign of  $d_{ijk}^{\rm (SC)}$  and  $q_0$ . We stress that this interpretation is valid even for the monopole state.

Furthermore,  $d_{ijk}^{(\text{SC})}$  and  $q_0$  show a similar peak structure around  $\alpha=\pm0.2$  and drastically change around  $\beta = \pm 1$ . These behaviors are related to the density of states (DOS) in the low-energy region, which is shown for the  $A_q + iB_{3u}$  anapole state with several parameters (Fig. 3). Note that the DOS in Fig. 3 is calculated with  $q_0 = 0$  for simplicity. Parameters leading to larger DOS around the Fermi level E=0 correspond to larger  $q_0$  and  $d_{ijk}^{(SC)}$ . This is consistent with the fact that the asymmetric spectrum is the main source of both  $q_0$  and  $d_{ijk}^{\rm (SC)}$ . It is also indicated that thermally excited quasiparticles are essential. In Fig. 3, we see that the low-energy Bogoliubov spectrum is sensitive to the parameter  $\beta$ . With our parameter set, the spectrum is fully-gapped for  $|\beta| < 1$ while the nodal spectrum appears with  $|\beta| \geq 1$ . To be more precise, point nodes are present at  $\beta = 1$ , and when  $\beta > 1$ , the Bogoliubov Fermi surface appears (see Appendix B), which has been studied with interest in the topological nature [64–66]. Thus, the low-energy DOS increases for  $\beta \geq 1$ , and therefore, the SCPE and Cooper pairs' momentum are enhanced.

Based on the above discussion, we expect a notable temperature dependence reflecting the gap structure. Indeed, a characteristic behavior is observed in the temperature dependence of  $q_0$  and  $d_{ijk}^{\rm (SC)}$ , which are suppressed in the low-temperature region (Fig. 4). In Ref. [38], it is shown that the asymmetry of the Bogoliubov spectrum is reflected in the anapole moment through the Fermi distribution function as  $f(E(\mathbf{k})) - f(E(-\mathbf{k}))$ , and therefore, the anapole moment and  $q_0$  are suppressed in the low-temperature region of gapped states. The SCPE is expected to be suppressed by the same mechanism. Indeed, the SCPE shows exponential temperature dependence of the structure of the structure dependence of  $q_0$  are suppressed by the same mechanism.

dence in the full-gapped state ( $\beta=0.7$ ) while it shows power-law dependence in the nodal state ( $\beta=1$ ). These results support the fact that the SCPE in the group velocity model relies on the asymmetric energy spectrum, like the magnetopiezoelectric effect in the odd-parity magnetic ordered states [36, 62, 63]. Hereafter, we call this mechanism of SCPE 'asymmetric origin' named after the asymmetric Bogoliubov spectrum.

#### (2) Geometric effect model

Second, we set  $\alpha_y = -\alpha_x (= -\alpha)$  and  $\beta = 0$ , in which the origin of the effective anapole moment is the geometric term since the group velocity term disappears. Note that the point group of the monopole superconducting state with this parameter set is  $D_4$ , leading to the constraints  $d_{xyz}^{(SC)} = 0$  and  $d_{yzx}^{(SC)} = -d_{zxy}^{(SC)}$ .

straints  $d_{xyz}^{(\mathrm{SC})} = 0$  and  $d_{yzx}^{(\mathrm{SC})} = -d_{zzy}^{(\mathrm{SC})}$ . The  $\alpha$  dependence of  $q_0$  and  $d_{ijk}^{(\mathrm{SC})}$  is shown in Fig. 5, which reveals the finite SCPE in the geometric effect However, in contrast to the group velocity model, the Bogoliubov spectrum is symmetric in this model for  $q_0 = 0$  (see Appendix C). Indeed,  $q_0 = 0$  in the monopole state and the spectrum is symmetric as  $E_{\alpha}(\mathbf{k}) = E_{\alpha}(-\mathbf{k})$ . Therefore, the origin of the SCPE must be different from the group velocity model where the asymmetric spectrum causes the SCPE. The geometric effect model also shows a similar parameter dependence of the Cooper pairs' momentum and the SCPE coefficients. Considering the fact that the anapole moment arises from the quantum geometry in this model [38], the similarity implies that the quantum geometry plays an essential role also in the SCPE. The  $\alpha$  symmetric behavior of the SCPE coefficients  $d_{ijk}^{(SC)}$  is consistent with this interpretation because the quantum geometry induces the  $\alpha$  symmetric anapole moment in the geometric effect model model [38].

The above discussion is supported by the temperature dependence of  $q_0$  and  $d_{ijk}^{\rm (SC)}$  plotted in Fig. 6. Although there is a sizable energy gap in the spectrum (see Appendix C), the SCPE and Cooper pairs' momentum are sizable even at low temperatures, in contrast to the group velocity model (Fig. 4). Indeed, the temperature dependence of  $q_0$  and  $d_{ijk}^{\rm (SC)}$  are weak. This behavior is consistent with the above discussion because the effect of the quantum geometry of Bloch electrons is not suppressed by the energy gap. Hereafter, we call this case of the SCPE 'symmetric origin' named after the symmetric Bogoliubov spectrum.

#### (3) Mixed model

Finally, we set  $\alpha_y = -\alpha_x (= -\alpha)$  and  $\beta \neq 0$ , where both the group velocity term and the geometric term contribute to the effective anapole moment. As shown in Fig. 7, the  $\alpha$  dependence of  $q_0$  and  $d_{ijk}^{(SC)}$  is asymmetric

for  $\beta=1$ , although it is almost symmetric for  $\beta=0.7$ . We can interpret these features based on the results in the previous subsections: Since  $q_0$  and  $d_{ijk}^{\rm (SC)}$  are very small in the group velocity model for  $|\beta|<1$  (Fig. 2), the SCPE of the asymmetric origin is naturally small in the mixed model. Thus, the SCPE mainly arises from the symmetric origin, consistent with the  $\alpha$ -symmetric behavior similar to the geometric effect model (Fig. 5). On the other hand, the asymmetric origin gives rise to a sizable contribution to the SCPE when  $|\beta| \geq 1$ , making the SCPE asymmetric with respect to  $\alpha$ .

As we discussed for the group velocity model, the SCPE of the asymmetric origin is related to the DOS. This is correct in the mixed model as well. Figure 8 shows the DOS in the mixed model. First, we see that the superconducting gap suppresses the low-energy DOS for  $\beta=0.7$ , consistent with the negligible contribution to the SCPE by the asymmetric origin. Second, we see sizable DOS for  $\beta=1$ , and it is larger for  $\alpha=-0.4$  than for  $\alpha=0.4$ . Thus, it is indicated that the SCPE of the asymmetric origin is suppressed for  $\alpha>0$  because of the small low-energy DOS. In other words, we see a significant contribution of the asymmetric origin when  $\beta\geq 1$  and  $\alpha<0$ . This is consistent with the parameter dependence of the SCPE in Fig. 7.

The  $\beta$  dependence also supports the above discussion. Note that the parameter sets  $(\alpha_x, \alpha_y, \beta)$  and  $(-\alpha_x, -\alpha_y, -\beta)$  give the same results in our model. Fig. 9 shows the  $\beta$  dependence of the SCPE coefficients for  $\alpha = 0.4$ . The drastic change around  $\beta = -1$  is attributed to the sizable DOS, which is equivalent to that for  $(\alpha, \beta) = (-0.4, 1)$ . Figure 9 also reveals that the SCPE of the symmetric origin is nearly  $\beta$ -independent.

The SCPE in the mixed model may show a unique temperature dependence as a consequence of the competition between the asymmetric and symmetric origins. As shown in Figs. 10(a) and 10(c),  $q_0$  and  $d_{yzx}^{(SC)}$  change the sign at a certain temperature. The sign reversal occurs because the temperature dependence is significantly different between the SCPE of the asymmetric origin and that of the symmetric origin (compare Fig. 4 with Fig. 6). When the superconducting state is gapped, the SCPE is dominated by the symmetric origin at low temperatures, and thus, the quantum geometry is expected to play an essential role. On the other hand, the asymmetric origin related to the asymmetric Bogoliubov spectrum gives a large contribution near the transition temperature, and it can cause the sign change. Note that the sign reversal is not a general property, and it is sensitive to the detail of the system and SCPE mode. Indeed, there is no sign change in  $d_{xxx}^{(SC)}$  (see Fig. 10(b)), for instance.

It should be noticed that the Cooper pairs' momentum  $q_0$  and the SCPE coefficients  $d_{ijk}^{\rm (SC)}$  show similar behaviors in all the models and parameters studied in this paper. This is also the case of the helical superconducting state studied earlier [43]. Surprisingly, this correspondence applies to the SCPE in the monopole supercon-

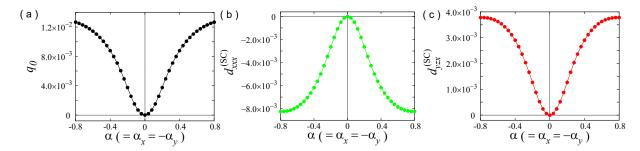


FIG. 5. Results of the geometric effect model:  $\alpha$  dependence of (a)  $q_0$ , (b)  $d_{xxx}^{(SC)}$  in the  $A_g + iB_{3u}$  anapole state, and (c)  $d_{yzx}^{(SC)}$  in the  $A_g + iA_u$  monopole state. We set  $\alpha = \alpha_x = -\alpha_y$ ,  $\beta = 0$  and T = 0.01.

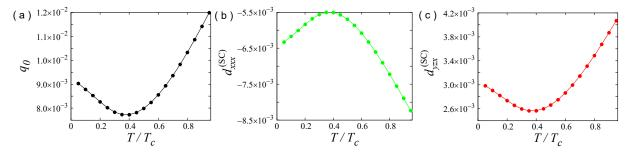


FIG. 6. Results of the geometric effect model: temperature dependence of (a)  $q_0$ , (b)  $d_{xxx}^{(SC)}$  in the  $A_g + iB_{3u}$  anapole state, and (c)  $d_{yzx}^{(SC)}$  in the  $A_g + iA_u$  monopole state. We set  $\alpha = \alpha_x = -\alpha_y = 0.4$  and  $\beta = 0$ .

ducting state as well. Although  $q_0 = 0$  in the monopole state, the SCPE shows a similar parameter dependence to  $q_0$  in the anapole state. From these results, we suppose that the SCPE arises from the asymmetric Bogoliubov spectrum and quantum geometry like the anapole moment [38]. Further analysis of the SCPE related to quantum geometry is left as a future issue.

#### IV. FIELD-FREE DIODE EFFECT

In this section, we demonstrate the field-free SDE in the anapole superconductors, which means the nonreciprocity in the critical current in the absence of the magnetic field. Here, we consider the SDE along the x-axis with the  $A_g + iB_{3u}$  anapole superconducting state in mind. Adopting the formulation for the intrinsic SDE [19], we calculate the depairing critical current as

$$J_{c+} = \max_{q_x} \langle \hat{J}_x \rangle_{eq,q_x}, \quad J_{c-} = \min_{q_x} \langle \hat{J}_x \rangle_{eq,q_x}, \quad (14)$$

using Eq. (11). The  $q_x$  dependence of  $\langle \hat{J}_x \rangle_{\text{eq},q_x}$  in the  $A_g + iB_{3u}$  anapole state is shown in Fig. 11 for example, by which we determine  $J_{c+}$  and  $J_{c-}$ . The nonreciprocal component of the critical current is given by

$$\Delta J_{\rm c} = J_{\rm c+} + J_{\rm c-},$$
 (15)

and the SDE efficiency is defined as

$$r = \Delta J_{\rm c}/\bar{J}_{\rm c},\tag{16}$$

with 
$$\bar{J}_{c} = (J_{c+} - J_{c-})/2$$
.

The numerical results of  $\Delta J_{\rm c}$  and r are shown in Figs. 12 and 13, respectively. We obtain finite nonreciprocity in the critical current characterized by  $\Delta J_c$ and r in all the models for the anapole superconducting states, namely, the (1) group velocity model, (2) geometric effect model, and (3) mixed model. Thus, the fieldfree SDE is a ubiquitous feature of anapole superconductors. It is shown that  $\Delta J_{\rm c}$  is suppressed monotonically with increasing temperature. This behavior is in stark contrast to the fact that the temperature dependence of Cooper pairs' momentum  $q_0$  and SCPE coefficients significantly depends on the model. Note that the temperature scaling around  $T = T_c$  is not reliable because the qdependence of the magnitude of gap function is neglected in our calculation, while it is negligible and the results are reliable at low temperatures [19]. Interestingly, the SDE efficiency r reaches 40%, which is comparable to the maximum value in the helical superconducting state at high magnetic fields [19]. Thus, our results suggest a sizable SDE in the anapole superconducting state at the zero magnetic field.

The SDE along the x-axis is allowed only in the anapole state, and it vanishes in the monopole state. Generally speaking, the SDE occurs in the anapole state with supercurrent in the same direction as the Cooper pairs' momentum  $q_0$ . Therefore, the SDE is suitable as a probe to distinguish the anapole and monopole states and to determine the direction of the anapole moment.

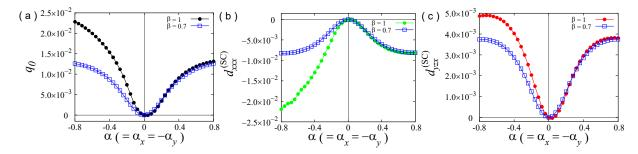


FIG. 7. Results of the mixed model:  $\alpha$  dependence of (a)  $q_0$ , (b)  $d_{xxx}^{(SC)}$  in the  $A_g + iB_{3u}$  anapole state, and (c)  $d_{yzx}^{(SC)}$  in the  $A_g + iA_u$  monopole state. We set  $\alpha = \alpha_x = -\alpha_y$ ,  $\beta = 1$  or 0.7, and T = 0.01.

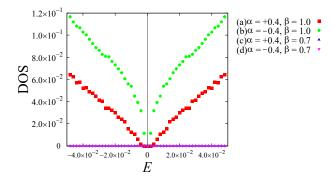


FIG. 8. The DOS in the  $A_g + iB_{3u}$  anapole state with the following parameters: (a)  $\alpha = +0.4$ ,  $\beta = 1$ , (b)  $\alpha = -0.4$ ,  $\beta = 1$ , (c)  $\alpha = +0.4$ ,  $\beta = 0.7$ , and (d)  $\alpha = -0.4$ ,  $\beta = 0.7$ . We set  $q_0 = 0$  for simplicity.

#### V. SUMMARY AND DISCUSSION

In this paper, we formulated and demonstrated the superconducting piezoelectric effect (SCPE) in the anapole and monopole superconducting states. We also showed the field-free superconducting diode effect (SDE) in the anapole superconducting state. The spontaneous IS and TRS breaking in these PT-symmetric superconducting states allows the off-diagonal and nonreciprocal responses without external symmetry-breaking fields. Therefore, the SCPE and SDE directly reflect the symmetry of superconducting states, and they can be used for probing the exotic symmetry and topology of superconductors. In particular, the SCPE occurs under all the symmetry groups lacking the IS and TRS. Thus, in principle, we can distinguish the symmetry of superconducting states by the analysis of the SCPE tensor. For instance, we provided the classification table for the SCPE tensor in the  $D_{2h}$  point group, corresponding to the candidate superconductor UTe<sub>2</sub>. On the other hand, the field-free SDE occurs only along the anapole moment in the anapole superconducting state. Therefore, the observation of the SDE may evidence the anapole superconductivity and determine the direction of the anapole moment.

Our calculations revealed the close relationship between the SCPE and the Cooper pairs' momentum. In the anapole state, the Cooper pairs can get finite momentum like in the FFLO and helical superconducting states, and the momentum is proportional to the anapole moment. In our results, the SCPE coefficients show similar parameter dependence to the Cooper pairs' momentum. According to our recent studies [37, 38], the anapole moment and Cooper pairs' momentum may have several origins, namely, the asymmetric spectrum of Bogoliubov quasiparticles and quantum geometry of Bloch electrons. The similarity implies the same origins of the SCPE. Interestingly, the relation is confirmed between the SCPE in the monopole state and Cooper pairs' momentum in the anapole state. To clarify the microscopic origin of the SCPE, further theoretical analysis is desired and remains to be a future issue.

On the other hand, the SDE looks unrelated to the Cooper pairs' momentum unlike the results of the helical superconducting state [19, 25]. Therefore, the SDE is unlikely to be used for a probe of the magnitude of Cooper pairs' momentum. A characteristic property of the anapole superconducting state is that the SDE occurs at the zero magnetic field. Such field-free SDE has been searched in the recent research of SDE, but the platform is limited at present [14–16, 23]. Anapole superconductors are a platform of field-free SDE without symmetry-breaking magnetic order or external fields. The rectified supercurrent is parallel to the momentum of Cooper pairs. In our calculation, a large SDE quality factor over 40% is obtained.

We expect that the SCPE and SDE will be complementary to other observable quantities characterizing the exotic superconducting stats. For instance, our recent work [38] proposed a phenomenon specific to the anapole superconductor, the temperature-dependent Bogoliubov Fermi surface. The Bogoliubov Fermi surface affects thermodynamic properties [67–69], which could be experimentally verified, in principle. On the other hand, the SCPE and SDE occur regardless of the presence or absence of the Bogoliubov Fermi surface.

An intriguing future task is to examine the SCPE and SDE in UTe<sub>2</sub>, a candidate of the anapole and monopole superconductivity. A recent ultrasound measurement detected softening of the elastic mode corresponding to the strain  $s_{zx}$  [70]. Thus, it is expected that the corresponding SCPE mode is enhanced. That is the  $B_1$  mode in

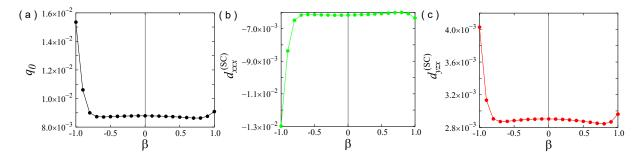


FIG. 9. Results of the mixed model:  $\beta$  dependence of (a)  $q_0$ , (b)  $d_{xxx}^{(\text{SC})}$  in the  $A_g + iB_{3u}$  anapole state, and (c)  $d_{yzx}^{(\text{SC})}$  in the  $A_g + iA_u$  monopole state. We set  $\alpha = \alpha_x = -\alpha_y = 0.4$  and T = 0.01.

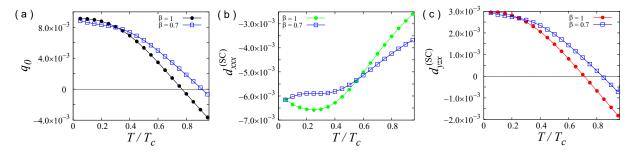


FIG. 10. Results of the mixed model: temperature dependence of (a)  $q_0$ , (b)  $d_{xxx}^{(SC)}$  in the  $A_g + iB_{3u}$  anapole state, and (c)  $d_{yzx}^{(SC)}$  in the  $A_g + iA_u$  monopole state. We set  $\alpha = \alpha_x = -\alpha_y = 0.4$  and  $\beta = 1$  or 0.7.

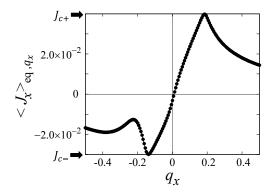


FIG. 11. Supercurrent  $\langle \hat{J}_x \rangle_{\text{eq},q_x}$  as a function of  $q_x$  in the mixed model of the  $A_g + iB_{3u}$  anapole state. We set  $\alpha = \alpha_x = -\alpha_y = 0.4$ ,  $\beta = 1$ , and T = 0.01. Critical currents  $J_{c+}$  and  $J_{c-}$  are marked by arrows.

the anapole superconducting state while  $B_2$  mode in the monopole superconducting state. The former is induced by the supercurrent along the z-axis, and it is along the y-axis in the latter.

#### ACKNOWLEDGMENTS

We thank A. Daido for fruitful discussion. This work was supported by JST SPRING (Grant Number JP-MJSP2110), JSPS KAKENHI (Grants No. JP18H01178, No. JP18H05227, No. JP20H05159, No. JP21K18145,

No. JP22H01181, No. JP22H04933, No. JP22J22520) and SPIRITS 2020 of Kyoto University.

# Appendix A: Symmetry analysis of PT-symmetric superconducting states and SCPE based on the point group $D_{2h}$

We discuss the anapole and monopole superconducting states classified based on the  $D_{2h}$  point group. There are four even-parity and four odd-parity irreducible representations in the  $D_{2h}$  point group, and accordingly, their coexistence allows sixteen mixed-parity superconducting states. The classification of superconducting states is summarized in Table III. In the mixed-parity superconducting states, the point group symmetry is reduced from the normal state point group  $(D_{2h})$  owing to the spontaneous parity violation. For instance, the point group of the  $B_{1q} + iB_{3u}$  state is  $C_{2v}$  with the principal axis in the y direction. This means that the  $B_{1g} + iB_{3u}$  state is an anapole superconducting state, where Cooper pairs can get total momentum in the y direction,  $\mathbf{q} = (0, q_0, 0)$ . In Table III, we represent  $C_{2v}(y)$  for such symmetry. The table reveals that the point group of parity-mixed superconducting states may be either  $C_{2v}(x)$ ,  $C_{2v}(y)$ ,  $C_{2v}(z)$ (anapole), or  $D_2$  (monopole). We have shown the SCPE mode in the  $C_{2v}(x)$  anapole and  $D_2$  monopole states in Tables I and II, respectively. For completeness, we show the possible SCPE mode in the  $C_{2v}(y)$  and  $C_{2v}(z)$ anapole superconducting states in Tables IV and V, re-

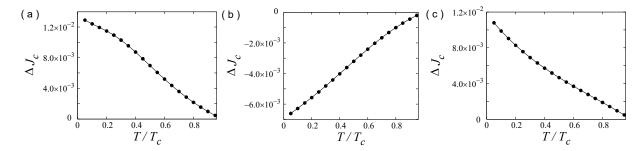


FIG. 12. Temperature dependence of the nonreciprocal critical current  $\Delta J_c$  in the (a) group velocity model, (b) geometric effect model, and (c) mixed model of the  $A_g + iB_{3u}$  anapole state. The parameters  $(\alpha, \beta)$  are (a) (0.4, 1), (b) (0.4, 0), and (c) (0.4, 1) as in Figs. 4, 6 and 10.

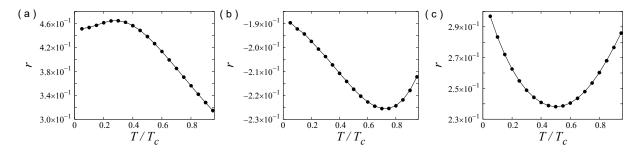


FIG. 13. Temperature dependence of the SDE efficiency r in the (a) group velocity model, (b) geometric effect model, and (c) mixed model of the  $A_g + iB_{3u}$  anapole state. The parameters  $(\alpha, \beta)$  are (a) (0.4, 1), (b) (0.4, 0), and (c) (0.4, 1) as in Figs. 4, 6 and 10.

spectively.

TABLE IV. List of the IRs of the  $C_{2v}(y)$  anapole superconducting state and corresponding strain  $s_{ij}$ , supercurrent  $J_k$ , and SCPE mode  $d_{ijk}^{(SC)}$ .

IR	Strain	Supercurrent	SCPE modes
$\overline{A_1}$	$s_{xx}, s_{yy}, s_{zz}$	$J_y$	$d_{xxy}^{(SC)} \ d_{yyy}^{(SC)} \ d_{zzy}^{(SC)}$
$\overline{A_2}$	$s_{zx}$	_	_
$B_1$	$s_{xy}$	$J_x$	$d_{xyx}^{(\mathrm{SC})}$
$B_2$	$s_{yz}$	$J_z$	$d_{yzz}^{ m (SC)}$

TABLE V. List of the IRs of the  $C_{2v}(z)$  anapole superconducting state and corresponding strain  $s_{ij}$ , supercurrent  $J_k$ , and SCPE mode  $d_{ijk}^{(SC)}$ .

IR	Strain	Supercurrent	SCPE modes
$\overline{A_1}$	$s_{xx}, s_{yy}, s_{zz}$	$J_z$	$d_{xxz}^{(SC)} d_{yyz}^{(SC)} d_{zzz}^{(SC)}$
$\overline{A_2}$	$s_{xy}$	_	_
$B_1$	$s_{yz}$	$J_y$	$d_{yzy}^{(\mathrm{SC})}$
$B_2$	$s_{zx}$	$J_x$	$d_{zxx}^{(SC)}$

We here comment on the derivation of the possible SCPE modes. Tables  $I,\,II,\,IV,\,$  and V are obtained by considering the condition that the supercurrent and strain

belong to the same irreducible representation. An alternative way is to consider the compatible relation of irreducible representations. Because the SCPE tensor  $d_{ijk}^{\rm (SC)}$  becomes finite with the reduction of the symmetry of the system,  $d_{ijk}^{\rm (SC)}$  must belong to the totally symmetric representation in the superconducting state and not in the normal state. When we apply this condition to the  $D_{2h}$  point group, we find that finite SCPE coefficients  $d_{ijk}^{\rm (SC)}$  belong to the  $B_{3u}$  ( $A_u$ ) irreducible representation in the  $A_g+iB_{3u}$  anapole ( $A_g+iA_u$  monopole) state.

### Appendix B: Analysis of the group velocity model

In this Appendix, we show some notable properties of the group velocity model. First, we show the Bogoliubov spectrum in Fig. 14 assuming Cooper pairs' momentum  $q_0=0$ . The spectrum is asymmetric in the  $k_x$  direction and the asymmetry is reversed by changing the sign of the ASOC,  $\alpha_x$  (see the spectrum for  $k_y=\pi/4$ ). This property results in the  $\alpha$ -antisymmetric behavior of the SCPE and  $q_0$  in the group velocity model. Their  $\beta$ -antisymmetric behavior is also explained in the same way.

Next, we discuss the gap structure. Note that the spectrum is symmetric on the  $k_y=0$  and  $k_y=\pi$  planes if we set  $q_0=0$  (see Fig. 14 for  $k_y=0$ ). The analytic representation of the Bogoliubov spectrum on these planes is

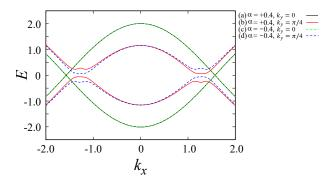


FIG. 14. The spectrum of Bogoliubov quasiparticles in the group velocity model for the  $A_g+iB_{3u}$  anapole state. We show the energy dispersion along the  $k_x$  axis by setting  $k_z=0$  and (a),(c)  $k_y=0$  or (b),(d)  $k_y=\pi/4$ . The spectrum with  $k_y=0$  is gapless. (a),(b) The solid lines represent the spectrum calculated with  $\alpha_x=0.4$ , while (c),(d) the dashed lines are obtained with  $\alpha_x=-0.4$ . We assume  $\alpha_y=0$ ,  $\beta=1$ , T=0.01 and set  $q_0=0$ .

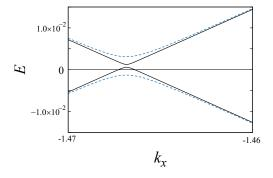


FIG. 15. The same plot as Fig. 14. The black solid (blue dashed) line shows the result for  $\alpha_x=0.4$  and  $\beta=1.01$  ( $\beta=1$ ). We set  $k_y=-0.0481$  and  $k_z=-0.457$  to show a part of the Bogoliubov Fermi surface.

obtained as

$$E(\mathbf{k}) = \pm \sqrt{(\varepsilon_{\mathbf{k}} - \mu)^2 + (\left|\Delta_{\mathbf{k}}^+\right| \pm \beta \Delta_1 d_y^g)^2}, \quad (B1)$$

where  $\Delta_{\mathbf{k}}^+ = \Delta_1 \psi^g + \Delta_2 d_z^u$ . There are nodes in the superconducting gap when  $\varepsilon_{\mathbf{k}} - \mu = 0$  and  $|\Delta_{\mathbf{k}}^+| \pm \beta \Delta_1 d_y^g = 0$ are simultaneously satisfied on the planes. Indeed, for  $\beta = 1$ , the point node is present on the  $k_y = 0$  plane, as we see in Fig. 14. When  $\beta > 1$ , Bogoliubov Fermi surfaces appear in several regions of the Brillouin zone. For instance, Fig. 15 shows the Bogoliubov spectrum indicating the Bogoliubov Fermi surface for  $\beta = 1.01$ . Thus, the superconducting gap structure significantly changes around  $\beta = \pm 1$ . This is the reason why the SCPE and  $q_0$  show remarkable  $\beta$  dependence around  $\beta = \pm 1$  in the group velocity model.

## Appendix C: Bogoliubov spectrum in the geometric effect model

Here, we show the energy spectrum of Bogoliubov quasiparticles in the geometric effect model. The spectrum without  $q_0$  can be analytically calculated and obtained as

$$E(\mathbf{k}) = \pm \sqrt{\left(\left|g_{\mathbf{k}}^{+}\right| \pm \sqrt{(\varepsilon_{\mathbf{k}} - \mu)^{2} + (\operatorname{Im}\Delta_{\mathbf{k}}^{+})^{2}}\right)^{2} + \left(\operatorname{Re}\Delta_{\mathbf{k}}^{+}\right)^{2}},$$
(C1)

where  $g_{\mathbf{k}}^{+} = g_x + ig_y$ . We confirm that the spectrum is symmetric for  $\mathbf{k}$ , i.e.  $E(\mathbf{k}) = E(-\mathbf{k})$  in contrast to the group velocity model. In addition, since  $\text{Re}\Delta_{\mathbf{k}}^{+} = \Delta_1 \psi^g > 0$  is always finite in our model, gap nodes are absent at least for  $q_0 = 0$ , Indeed, we see the gapped spectrum in Fig. 16.

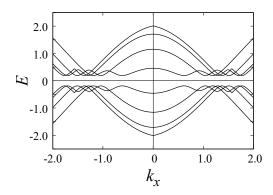


FIG. 16. The Bogoliubov spectrum of the  $A_g + iB_{3u}$  state with  $\alpha_x = -\alpha_y = 0.4$ ,  $\beta = 0$  (geometric effect model), and T = 0.01. We draw the spectrum on  $k_z = 0$  and  $k_y = 0, \pi/8, \pi/4, 3\pi/8$ .

<sup>[1]</sup> R. Wakatsuki, Y. Saito, S. Hoshino, Y. M. Itahashi, T. Ideue, M. Ezawa, Y. Iwasa, and N. Nagaosa, Sci. Adv. 3, e1602390 (2017).

<sup>[2]</sup> R. Wakatsuki and N. Nagaosa, Phys. Rev. Lett. 121, 026601 (2018).

<sup>[3]</sup> S. Hoshino, R. Wakatsuki, K. Hamamoto, and N. Nagaosa, Phys. Rev. B 98, 054510 (2018).

<sup>[4]</sup> Y. M. Itahashi, T. Ideue, Y. Saito, S. Shimizu, T. Ouchi, T. Nojima, and Y. Iwasa, Sci. Adv. 6, eaay9120 (2020).

<sup>[5]</sup> T. Schumann, L. Galletti, H. Jeong, K. Ahadi, W. M. Strickland, S. Salmani-Rezaie, and S. Stemmer, Phys. Rev. B 101, 100503 (2020).

<sup>[6]</sup> S. Nakamura, K. Katsumi, H. Terai, and R. Shimano, Phys. Rev. Lett. 125, 097004 (2020).

<sup>[7]</sup> Y. Miyasaka, R. Kawarazaki, H. Narita, F. Ando, Y. Ikeda, R. Hisatomi, A. Daido, Y. Shiota, T. Moriyama, Y. Yanase, and T. Ono, Applied Physics Express 14, 073003 (2021).

- [8] H. Watanabe, A. Daido, and Y. Yanase, Phys. Rev. B 105, 024308 (2022).
- [9] H. Watanabe, A. Daido, and Y. Yanase, Phys. Rev. B 105, L100504 (2022).
- [10] F. Ando, Y. Miyasaka, T. Li, J. Ishizuka, T. Arakawa, Y. Shiota, T. Moriyama, Y. Yanase, and T. Ono, Nature 584, 373 (2020).
- [11] Y.-Y. Lyu, J. Jiang, Y.-L. Wang, Z.-L. Xiao, S. Dong, Q.-H. Chen, M. V. Milošević, H. Wang, R. Divan, J. E. Pearson, P. Wu, F. M. Peeters, and W.-K. Kwok, Nature Communications 12, 2703 (2021).
- [12] L. Bauriedl, C. Bäuml, L. Fuchs, C. Baumgartner, N. Paulik, J. M. Bauer, K.-Q. Lin, J. M. Lupton, T. Taniguchi, K. Watanabe, C. Strunk, and N. Paradiso, Nature Communications 13, 4266 (2022).
- [13] C. Baumgartner, L. Fuchs, A. Costa, S. Reinhardt, S. Gronin, G. C. Gardner, T. Lindemann, M. J. Manfra, P. E. Faria Junior, D. Kochan, J. Fabian, N. Paradiso, and C. Strunk, Nature Nanotechnology 17, 39 (2022).
- [14] H. Wu, Y. Wang, Y. Xu, P. K. Sivakumar, C. Pasco, U. Filippozzi, S. S. P. Parkin, Y.-J. Zeng, T. McQueen, and M. N. Ali, Nature 604, 653 (2022).
- [15] H. Narita, J. Ishizuka, R. Kawarazaki, D. Kan, Y. Shiota, T. Moriyama, Y. Shimakawa, A. V. Ognev, A. S. Samardak, Y. Yanase, and T. Ono, Nature Nanotechnology 17, 823 (2022).
- [16] J.-X. Lin, P. Siriviboon, H. D. Scammell, S. Liu, D. Rhodes, K. Watanabe, T. Taniguchi, J. Hone, M. S. Scheurer, and J. I. A. Li, Nature Physics 18, 1221 (2022).
- [17] A. A. Kopasov, A. G. Kutlin, and A. S. Mel'nikov, Phys. Rev. B 103, 144520 (2021).
- [18] N. F. Q. Yuan and L. Fu, Proceedings of the National Academy of Sciences 119, e2119548119 (2022).
- [19] A. Daido, Y. Ikeda, and Y. Yanase, Phys. Rev. Lett. 128, 037001 (2022).
- [20] J. J. He, Y. Tanaka, and N. Nagaosa, New Journal of Physics 24, 053014 (2022).
- [21] S. Ilić and F. S. Bergeret, Phys. Rev. Lett. 128, 177001 (2022).
- [22] H. F. Legg, D. Loss, and J. Klinovaja, Phys. Rev. B 106, 104501 (2022).
- [23] H. D. Scammell, J. I. A. Li, and M. S. Scheurer, 2D Materials 9, 025027 (2022).
- [24] J. Jiang, M. Milošević, Y.-L. Wang, Z.-L. Xiao, F. Peeters, and Q.-H. Chen, Phys. Rev. Applied 18, 034064 (2022).
- [25] A. Daido and Y. Yanase, arXiv:2209.03515.
- [26] R. Kawarazaki, H. Narita, Y. Miyasaka, Y. Ikeda, R. Hisatomi, A. Daido, Y. Shiota, T. Moriyama, Y. Yanase, A. V. Ognev, A. S. Samardak, and T. Ono, Appl. Phys. Express 15, 113001 (2022).
- [27] J. Ishizuka and Y. Yanase, Phys. Rev. B 103, 094504 (2021).
- [28] S. Ran, I.-L. Liu, Y. S. Eo, D. J. Campbell, P. M. Neves, W. T. Fuhrman, S. R. Saha, C. Eckberg, H. Kim, D. Graf, F. Balakirev, J. Singleton, J. Paglione, and N. P. Butch, Nature Physics 15, 1250 (2019).
- [29] D. Braithwaite, M. Vališka, G. Knebel, G. Lapertot, J.-P. Brison, A. Pourret, M. E. Zhitomirsky, J. Flouquet, F. Honda, and D. Aoki, Communications Physics 2, 147 (2019).
- [30] D. Aoki, F. Honda, G. Knebel, D. Braithwaite, A. Nakamura, D. Li, Y. Homma, Y. Shimizu, Y. J. Sato, J.-P. Brison, and J. Flouquet, J. Phys. Soc. Japan 89, 053705

- (2020).
- [31] D. Aoki, J.-P. Brison, J. Flouquet, K. Ishida, G. Knebel, Y. Tokunaga, and Y. Yanase, Journal of Physics: Condensed Matter 34, 243002 (2022).
- [32] A. Rosuel, C. Marcenat, G. Knebel, T. Klein, A. Pourret, N. Marquardt, Q. Niu, S. Rousseau, A. Demuer, G. Seyfarth, G. Lapertot, D. Aoki, D. Braithwaite, J. Flouquet, and J.-P. Brison, arXiv:2205.04524.
- [33] K. Kinjo, H. Fujibayashi, S. Kitagawa, K. Ishida, Y. Tokunaga, H. Sakai, S. Kambe, A. Nakamura, Y. Shimizu, Y. Homma, D. X. Li, F. Honda, D. Aoki, K. Hiraki, M. Kimata, and T. Sasaki, arXiv:2206.02444.
- [34] H. Sakai, Y. Tokiwa, P. Opletal, M. Kimata, S. Awaji, T. Sasaki, D. Aoki, S. Kambe, Y. Tokunaga, and Y. Haga, arXiv:2210.05909.
- [35] Y. Wang and L. Fu, Phys. Rev. Lett. 119, 187003 (2017).
- [36] H. Watanabe and Y. Yanase, Phys. Rev. B 96, 064432 (2017).
- [37] S. Kanasugi and Y. Yanase, Commun. Phys. 5, 39 (2022).
- [38] T. Kitamura, S. Kanasugi, M. Chazono, and Y. Yanase, arXiv:2210.01399.
- [39] P. Fulde and R. A. Ferrell, Phys. Rev. 135, A550 (1964).
- [40] A. I. Larkin and Y. N. Ovchinnikov, Zh. Eksp. Teor. Fiz. 47, 1136 (1964).
- [41] E. Bauer and M. Sigrist, Non-centrosymmetric superconductors: introduction and overview (Springer, Heidelberg, 2012).
- [42] M. Smidman, M. B. Salamon, H. Q. Yuan, and D. F. Agterberg, Rep. Prog. Phys. 80, 036501 (2017).
- [43] M. Chazono, H. Watanabe, and Y. Yanase, Phys. Rev. B 105, 024509 (2022).
- [44] M. H. Fischer, M. Sigrist, D. F. Agterberg, and Y. Yanase, Annual Review of Condensed Matter Physics 14 (2023).
- [45] H. Watanabe and Y. Yanase, Phys. Rev. B 98, 245129 (2018).
- [46] N. Marzari and D. Vanderbilt, Phys. Rev. B 56, 12847 (1997).
- [47] R. Resta, Eur. Phys. J. B 79, 121 (2011).
- [48] S. Peotta and P. Törmä, Nature Communications 6, 8944 (2015).
- [49] L. Liang, T. I. Vanhala, S. Peotta, T. Siro, A. Harju, and P. Törmä, Phys. Rev. B 95, 024515 (2017).
- [50] P. Törmä, S. Peotta, and B. A. Bernevig, Nature Reviews Physics 4, 528 (2022).
- [51] Y. Gao, S. A. Yang, and Q. Niu, Phys. Rev. Lett. 112, 166601 (2014).
- [52] Y. Gao and D. Xiao, Phys. Rev. Lett. 122, 227402 (2019).
- [53] M. F. Lapa and T. L. Hughes, Phys. Rev. B 99, 121111 (2019).
- [54] A. Daido, A. Shitade, and Y. Yanase, Phys. Rev. B 102, 235149 (2020).
- [55] A. Julku, G. M. Bruun, and P. Törmä, Phys. Rev. B 104, 144507 (2021).
- [56] A. Julku, G. M. Bruun, and P. Törmä, Phys. Rev. Lett. 127, 170404 (2021).
- [57] J. Ahn, G.-Y. Guo, and N. Nagaosa, Phys. Rev. X **10**, 041041 (2020).
- [58] H. Watanabe and Y. Yanase, Phys. Rev. X 11, 011001 (2021).
- [59] J.-W. Rhim, K. Kim, and B.-J. Yang, Nature 584, 59 (2020).
- [60] D. D. Solnyshkov, C. Leblanc, L. Bessonart, A. Nalitov, J. Ren, Q. Liao, F. Li, and G. Malpuech, Phys. Rev. B

- **103**, 125302 (2021).
- [61] Q. Liao, C. Leblanc, J. Ren, F. Li, Y. Li, D. Solnyshkov, G. Malpuech, J. Yao, and H. Fu, Phys. Rev. Lett. 127, 107402 (2021).
- [62] Y. Shiomi, H. Watanabe, H. Masuda, H. Takahashi, Y. Yanase, and S. Ishiwata, Phys. Rev. Lett. 122, 127207 (2019).
- [63] Y. Shiomi, H. Masuda, H. Takahashi, and S. Ishiwata, Sci. Rep. 10, 7574 (2020).
- [64] D. F. Agterberg, P. M. R. Brydon, and C. Timm, Phys. Rev. Lett. 118, 127001 (2017).
- [65] P. M. R. Brydon, D. F. Agterberg, H. Menke, and C. Timm, Phys. Rev. B 98, 224509 (2018).
- [66] J. M. Link and I. F. Herbut, Phys. Rev. Lett. 125, 237004 (2020).
- [67] S. Autti, J. T. Mäkinen, J. Rysti, G. E. Volovik, V. V. Zavjalov, and V. B. Eltsov, Phys. Rev. Research 2, 033013 (2020).
- [68] C. Setty, Y. Cao, A. Kreisel, S. Bhattacharyya, and P. J. Hirschfeld, Phys. Rev. B 102, 064504 (2020).
- [69] J. Ahn and N. Nagaosa, Nat. Commun. 12, 1617 (2021).
- [70] K. Ushida, T. Yanagisawa, R. Hibino, M. Matsuda, H. Hidaka, H. Amitsuka, G. Knebel, J. Flouquet, and D. Aoki, arXiv:2211.08354.